A SIMPLE PURE WATER OSCILLATOR

S. LAKSHMIVARAHAN, N. TRUNG, AND BARRY RUDDICK

Abstract. In this paper we analyze the properties of a pure water oscillator by considering the pure water lake as a well mixed two layered system. While there is heating of and evaporation from the shallow top layer, the temperature of the deep bottom layer is assumed to be constant. By exploiting the nonlinear dependence of the density of pure water on temperature, we describe two complementary mathematical models to capture the vertical instability resulting from the variation of the density of the top layer with temperature.

1. Introduction

Welander [11] was the first to analyze the properties of the so-called heat-salt oscillator by considering a well-mixed two layered system of sea water where there is heating and evaporation from the top layer and vertical turbulent mixing between the layers. Using a simple flip or threshold model consisting two – one for the evolution of the relative temperature and the other for that of relative salinity of the top layer with respect to the bottom layer, nonlinear, coupled system of ordinary differential equations (ODEs) with discontinuous right hand side to capture the vertical turbulent mixing, he demonstrated oscillations for certain values of parameters that control the vertical mixing. The nonlinear coupling is a direct consequence of the nonlinear dependence of the density $\rho(S,T)$ of the sea water on both salinity, S and temperature, T. Shortly thereafter, Ruddick and Zhang [9] using more realistic parameterizations, presented two complementary models, with continuous right hand sides proved that except in certain extreme cases, there cannot be oscillations. In the first model, they used a more realistic physics to capture the vertical turbulent mixing and in the second they used the "salt finger" formation to capture the vertical mixing. Both the approaches naturally lead to a system of two nonlinear coupled ODEs with continuous right-hand side. By invoking to the classical result due to Poincare – Bendixson, they showed that in the majority of cases, this system exhibited no oscillation.

In this paper, we examine the presence of oscillations in a system quite like the one described by Welander [11] and Ruddick and Zhang [9] with

the primary difference that the water is pure with no salt component. We are motivated by the observation relating to the overturning of water in pure water lakes that occurs when the seasons change from summer to autumn as the top layer cools and again from winter to spring when the top layer thaws. This overturning is largely a consequence of the nonlinear dependence of the density of pure water on its temperature. Our findings mirrors the developments in Welander [11] and Ruddick and Zhang [9].

Following Welander [11], in Section 2 we describe a class of flip-flop models consisting of a single nonlinear ODE with discontinuous right-hand side. We provide a complete characterization of bifurcation for the entire range of parameters that describe the vertical turbulent mixing and identify the regions that exhibit vertical oscillations. Motivated by the arguments in Ruddick and Zhang [9], in Section 3 we describe a model (based on more realistic parameterization, with continuous right-hand side) consisting of a single nonlinear ODE with three equilibria of which one is unstable and two are stable. The derivative of the (continuously differentiable) right-hand side (which are the eigenvalues of the Jacobian of the right-hand side) at the two stable equilibria differ by two orders of magnitude and hence this model is inherently stiff. Using special solvers for stiff system, it is shown that this latter class of models do not exhibit oscillation. Concluding remarks are in Section 4.

Nonlinear dependence of density on temperature is described in Appendix A. A resumé of the properties of piece-wise smooth dynamical system is contained in Appendix B. A discussion of the arrival time of the solution near the stable equilibrium is given in Appendix C. A realistic parameterization to capture the vertical turbulent mixing is given in Appendix D, which is the special case of the derivations in Ruddick and Zhang [9].

2. A Two Box Model

A fresh water lake can be conveniently modeled by a system of two well-mixed boxes arranged vertically as shown in the Figure 1. The shallow surface box of volume V_s $\left(m^3\right)$ is at a temperature T_s (°C). T_s varies due to the thermal interaction—Newtonian heating/cooling, between the atmosphere above at temperature $T_a \left(\gtrless T_s\right)$ and due to turbulent mixing with the deep box resulting from the static instability due to increased density of water in the surface box arising from the heat exchange with the atmosphere. The deep box is of volume V_d $\left(m^3\right)$ $\left(\gg V_s\right)$ and is assumed to be at a constant temperature T_d. The potential for the vertical oscillation in this system is largely a result of the nonlinear dependence of density $\rho\left(T\right)$ of the pure water on the temperature T as described in the Appendix A.

Accordingly the dynamics of evolution of T_s can be captured by the following ordinary differential equation

$$V_s \frac{\mathrm{d}\,(T_s - T_d)}{\mathrm{d}\,t} = C_T\,(T_a - T_s) - \gamma f\,(\Delta\rho)\,(T_s - T_d)\,, \tag{2.1}$$

where (it is assumed for definiteness that $T_a > T_s$) the first term on the right-hand side accounts for the heat exchange with atmosphere by Newtonian heating process and the constant C_T has units $m^3\,\mathrm{sec}^{-1}$. The second term on the right-hand side of (2.1) represents the heat exchange resulting from the flow where $\gamma f\,(\Delta\rho)$ is the measure of the flow in $m^3\,\mathrm{sec}^{-1}$, the normalized density difference $\Delta\rho = \Delta\rho\,(T_s)$ for simplicity in notation, the constant $\gamma\left(m^3\,\mathrm{sec}^{-1}\right)$ is known as the hydraulic constant and$f\,(\Delta\rho)$ is a monotonic non-decreasing function of $\Delta\rho$. Refer to Appendix A for characterization of $\Delta\rho$.

Dividing both sides by V_s, we get

$$\frac{\mathrm{d}\,(T_s - T_d)}{\mathrm{d}\,t} = k_T\,(T_a - T_s) - \eta f\,(\Delta\rho)\,(T_s - T_d)\,, \tag{2.2}$$

where $k_T = \frac{C_T}{V_s}\ \left(\mathrm{sec}^{-1}\right)$ is the reciprocal of the temperature relaxation time for the surface box and $\eta = \frac{\gamma}{V_s}\ \left(\mathrm{sec}^{-1}\right)$.

To capture the generic behavior of this model, we now non-dimensionalize the temperature and time as follows

$$x = \frac{T_s - T_d}{T_a - T_d} \quad \text{and} \quad s = \frac{t}{(1/k_T)}. \tag{2.3}$$

Substituting (2.3) into (2.2), since T_d is a constant, the latter becomes

$$\frac{\mathrm{d}\,x}{\mathrm{d}\,s} = (1 - x) - \overline{\eta} f\,(\Delta\overline{\rho}\,(x))\,x, \tag{2.4}$$

where

$$\overline{\eta} = \frac{\eta}{k_T} \tag{2.5}$$

is a non-dimensional parameter, and $\Delta\overline{\rho}\,(x)$ is the fractional density difference expressed in term of the non-dimensional temperature x. Refer to Appendix A for the transformation of the dependence of $\Delta\rho$ from T_s to x. By a clever choice of the function $\eta f\,(\Delta\rho)$, we can obtain quite a variety of models. In this note, following Welander [11], we consider the so called flip or threshold model.

2.1. **The Flip Model.** In this model, we define

$$\overline{\eta} f\,(\Delta\overline{\rho}\,(x)) = \begin{cases} k_0, & \text{if } \Delta\overline{\rho}\,(x) \le \varepsilon; \\ k_1, & \text{if } \Delta\overline{\rho}\,(x) > \varepsilon, \end{cases} \tag{2.6}$$

where $\varepsilon \ge 0$ is a small pre-specified threshold parameter and $k_0 \ll k_1$ are two constants that reflect the vertical turbulent heat-transfer resulting from

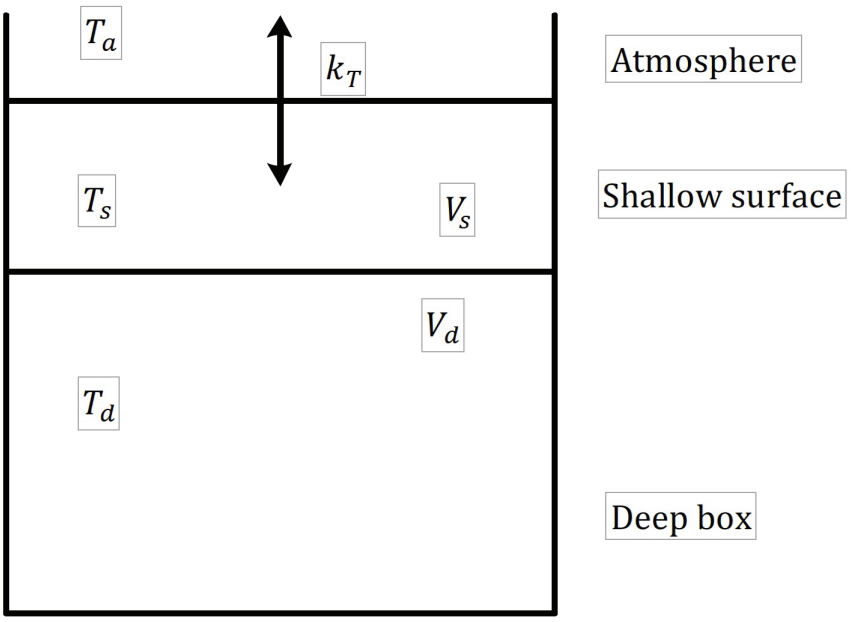

FIGURE 1. A 2-box model for the fresh water lake. The shallow surface box has volume V_s $\left(\mathrm{m}^3\right)$ and deep box has volume V_d $\left(\mathrm{m}^3\right)$ with $V_d \gg V_s$. It is assumed that $T_d = 2.0$.

the static instability induced by increasing density of the surface layer with temperature. An example of the range of temperature x where $\Delta\overline{\rho}(x) - \varepsilon > 0$ for $\varepsilon = 10^{-5}$ is given in Figure 2.

Define an indicator function

$$I_\varepsilon\left(\Delta\overline{\rho}(x)\right) = \begin{cases} 0, & \text{if } \Delta\overline{\rho}(x) \le \varepsilon; \\ 1, & \text{if } \Delta\overline{\rho}(x) > \varepsilon. \end{cases} \tag{2.7}$$

Combining (2.6) and (2.7), the model equation (2.4) can be written as

$$\frac{dx}{ds} = (1-x) - k_0 x - (k_1 - k_0)\, x I_\varepsilon\left(\Delta\overline{\rho}(x)\right), \tag{2.8}$$

or equivalently as

$$\frac{dx}{ds} = \begin{cases} f_1(x) = 1 - (1+k_0)\, x, & \text{if } \Delta\overline{\rho}(x) - \varepsilon \le 0; \\ f_2(x) = 1 - (1+k_1)\, x, & \text{if } \Delta\overline{\rho}(x) - \varepsilon > 0. \end{cases} \tag{2.9}$$

Clearly, this model equation has discontinuous right-hand side (DRHS) and the standard conditions for the existence and uniqueness of the solution are not satisfied. Filippov [3] presents an interesting extension of the notion of the solution of the ODE with DRHS, (Refer to Appendix B for a summary of Filipov's framework). There are essentially two ways to proceed. First is to apply Filippov's Theory to quantify the flow field near the points of discontinuity which guarantees the existence and uniqueness of the solution. A second and simpler approach is to invoke to the regularization method where we replace DRHS with a continuous approximation. In this note, while we follow Filipov's approach, for completeness, we also indicate a simple regularization method.

To this end, we can approximate a unit step function

$$I(y) = \begin{cases} 0, & \text{if } y \leq 0; \\ 1, & \text{if } y > 0, \end{cases} \tag{2.10}$$

by a continuous function of the form

$$H_\beta(y) = \frac{1}{2}\left[1 + \tanh(\beta y)\right], \tag{2.11}$$

where

$$\tanh(y) = \frac{e^y - e^{-y}}{e^y + e^{-y}}. \tag{2.12}$$

It is well-known that as β increases, the quality of approximation of the discontinuous function $I(y)$ in (2.10) by continuous function $H_\beta(y)$ in (2.11) steadily improves. Since $\Delta\overline{\rho}(x) - \varepsilon$ is of the order 10^{-4}, in the following, for better accuracy, we set $\beta = 10^6$.

Consequently, we can regularize the indicator function $I_\varepsilon(\Delta\overline{\rho}(x))$ in (2.9) by replacing it by $H_\beta(\Delta\overline{\rho}(x) - \varepsilon)$. Thus, the regularized version of the flip model is given by

$$\frac{dx}{ds} = f(x), \tag{2.13}$$

where

$$f(x) = (1-x) - k_0 x - (k_1 - k_0)\, x H_\beta(\Delta\overline{\rho}(x) - \varepsilon) \tag{2.14}$$

describes the flow field of this model dynamics.

3. Analysis

In this section we provide a complete catalog of the behavior of the model solution with respect to the choice of values of three parameters: ε, k_0 and k_1 in (2.9) and (2.14).

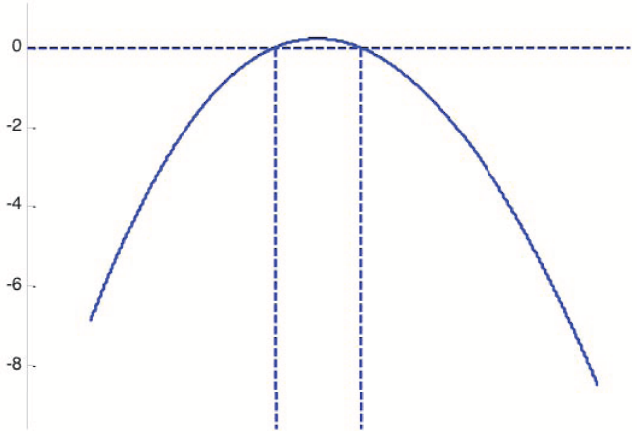

FIGURE 2. Plot of $\Delta\overline{\rho}\,(x) - \varepsilon$ for $\varepsilon = 10^{-5}$ $\Delta\overline{\rho}\,(x) - \varepsilon > 0$ when $x_1 \approx 0.0352 < x < x_2 \approx 0.3850$.

3.1. **Properties of $\Delta\overline{\rho}\,(x)$ and effect of ε.** From the definition of $\Delta\overline{\rho}\,(x)$ in (A.9) in the Appendix, the following properties readily follow.

P1) $\Delta\overline{\rho}\,(x)$ attains its maximum value of 3.2087×10^{-5} at $x = x_0 = 0.2086$.

P2) $\Delta\overline{\rho}\,(0) = 0$ and $\Delta\overline{\rho}\,(1) = -3.8778 \times 10^{-4}$.

P3) Setting $\varepsilon = 10^{-5}$, and solving the polynomial equation

$$\Delta\overline{\rho}\,(x) = \varepsilon$$

with real coefficients, we find that there are two real solutions at $x_1 \approx 0.0352$ and $x_2 \approx 0.3850$. Refer to Figure 2 for an illustration.

P4) $\Delta\overline{\rho}\,(x) - \varepsilon \geq 0$ for all $x_1 \leq x \leq x_2$, and $\Delta\overline{\rho}\,(x) - \varepsilon < 0$, otherwise.

P5) The separation between x_1 and x_2 measured by the distance $|x_2 - x_1|$ is an decreasing function of ε.

In the subsequent analysis, we fix $\varepsilon = 10^{-5}$. Stated in other words, the points of discontinuity in the flow field $f\,(x)$ in (2.9) occurs at x_1 and x_2 whose numerical value depends on the threshold parameter $\varepsilon \geq 0$. Further, since (3.1) is a polynomial with empirically determined real coefficients, the solution x_1 and x_2 of (3.1) in general are not rational numbers, hence

cannot be represented exactly by a terminating decimal expansion. Hence, for the flow field $f(x)$ of the threshold model (2.9) is given by $x_1 \approx 0.0352$ and $x_2 \approx 0.3850$.

$$f(x) = \begin{cases} f_1(x) = 1 - (1 + k_0)\, x, & \text{for } x \leq x_1 \text{ and } x \geq x_2, \\ f_2(x) = 1 - (1 + k_1)\, x, & \text{for } x_1 < x < x_2. \end{cases} \tag{3.1}$$

Against this background we now move on to analyzing the impact of the variation of parameters k_0 and k_1 on the flow field of the model dynamics.

3.2. **Analysis of Equilibria and Their Stability.** Analysis of the impact of the two parameters k_0 and k_1 on the model dynamics is largely a consequence of two facts:

(F1) $0 \leq k_0 < k_1$ and
(F2) both $f_1(x)$ and $f_2(x)$ in (3.1) are affine functions with negative slopes $-(1 + k_0)$ and $-(1 + k_1)$, respectively.

To fix the bearings, it is useful to refer to the plot of $f(x)$ in (3.1) with $k_0 = 0$ and $k_1 = 35$ in Figure 3. From the two facts listed above and a glance at Figure 3, we can easily verify the following relations between the values of $f_1(x)$ and $f_2(x)$ at the points of discontinuities, $x_1 \approx 0.0352$ and $x_2 \approx 0.3850$.

Since $0 \leq k_0 < k_1$, it follows that

(R1) $f_1(x_1) > f_2(x_1)$ and
(R2) $f_1(x_2) > f_2(x_2)$.

Since $f_1(x)$ and $f_2(x)$ are affine with negative slopes, from $x_1 < x_2$, it also follows that

(R3) $f_1(x_1) > f_1(x_2)$ and
(R4) $f_2(x_1) > f_2(x_2)$.

Given these four relations, there are eight other possibilities for the values of $f_i(x_1)$ and $f_i(x_2)$ for $i = 1,\ 2$. A complete listing of these eight possibilities and the conditions for their existence are given in Table 1.

Combining the four natural relations in (R1)–(R4) and eight conditions C1–C8 in Table 1, we now enlist a set of all six mutually exclusive combinations that provide a complete characterization of the model dynamics corresponding to various combinations of parameter ranges in Table 2. A partition of the 2-D parameter space for $k_1 \geq k_0 \geq 0$ induced by the six cases in Table 2 is given in Figure 4. The completeness of the six cases listed in Table 2 follows immediately from the fact that the union of the six partitions P_1 through P_6 is equal to the upper half $(k_1 \geq k_0)$ of the positive quadrant of the 2D plane.

For completeness, we present analogous results for the regularized version of $f(x)$ in (2.14) with $\beta = 10^6$ given in Table 4. It can be verified that

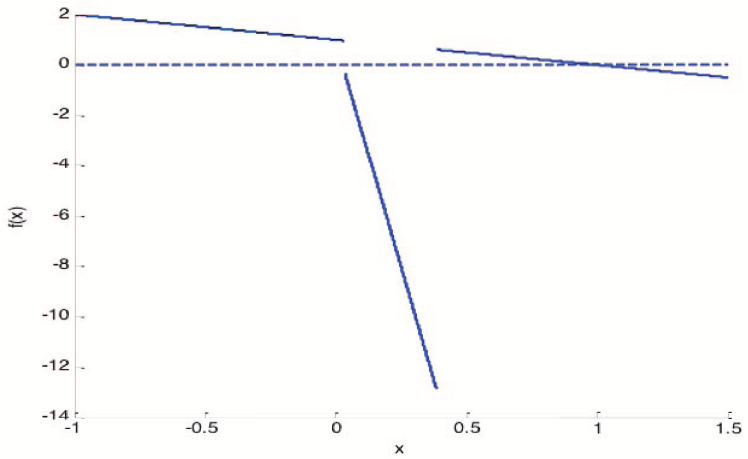

FIGURE 3. Plot of the $f(x)$ in (3.1) with $k_0 = 0$ and $k_1 = 35$.

TABLE 1. Conditions on the parameters k_0 and k_1 for the sign definiteness of $f_i(x_j)$ for $i = 1,\ 2$ and $j = 1,\ 2$ where $0 < x_1 < x_2$. Let $b = (1 - x_1)/(x_1)$ and $a = (1 - x_2)/(x_2)$. Given that $x_1 \approx 0.0352$ and $x_2 \approx 0.3850$, hence, $a \approx 1.597$ and $b \approx 27.409$.

Number	Property	Condition
C1	$f_1(x_1) > 0$	$k_0 < b$
C2	$f_1(x_1) < 0$	$k_0 > b$
C3	$f_2(x_1) > 0$	$k_1 < b$
C4	$f_2(x_1) < 0$	$k_1 > b$
C5	$f_1(x_2) > 0$	$k_0 < a$
C6	$f_1(x_2) < 0$	$k_0 > a$
C7	$f_2(x_2) > 0$	$k_1 < a$
C8	$f_2(x_2) < 0$	$k_1 > a$

entries in Table 4 converge to the corresponding entries in Table 3 as β increases.

To save space, a graphical view of the phase plot – plot of $f(x)$ in (3.1) vs. x along with the display of equilibria for only the first case in Table 3 are given in Figure 5.

TABLE 2. A listing of the set of all six mutually exclusive cases: $a = (1 - x_2)/(x_2) \approx 1.597$, $b = (1 - x_1)/(x_1) \approx 27.409$; $f_1 = f_1(x)$, $f_2 = f_2(x)$.

Case number	Condition at x_1	Condition at x_2	Condition on k_0 and k_1 defining the partition P_i
1	$f_1 > 0 > f_2$	$f_1 > 0 > f_2$	$P_1 : 0 \leq k_0 < a < b < k_1$
2	$f_1 > f_2 > 0$	$f_1 > 0 > f_2$	$P_2 : 0 \leq k_0 < a < k_1 < b$
3	$f_1 > f_2 > 0$	$f_1 > f_2 > 0$	$P_3 : 0 \leq k_0 < k_1 < a < b$
4	$0 > f_1 > f_2$	$0 > f_1 > f_2$	$P_4 : a < b < k_0 < k_1$
5	$f_1 > f_2 > 0$	$0 > f_1 > f_2$	$P_5 : a < k_0 < k_1 < b$
6	$f_1 > 0 > f_2$	$0 > f_1 > f_2$	$P_6 : a < k_0 < b < k_1$

It turns out that the set of all equilibria E_1 through E_{10} in Table 3 can be classified into two groups. First is the set of all six stable equilibria $S_1 = \{E_3,\ E_4,\ E_6,\ E_7,\ E_8,\ E_9\}$ that lie at a point of continuity of either $f_1(x)$ or $f_2(x)$ in (3.1). The second consisting of the rest of the four $S_2 = \{E_1,\ E_2,\ E_5,\ E_{10}\}$ that lie at the points of discontinuities x_1 and x_2 of $f(x)$ in (3.1).

According to the classical theory of ODE, a stable equilibrium of a smooth vector field is a local attractor in the sense that the solutions starting from its basin of attraction will eventually converge to this stable equilibrium point. The last column of Table 3 contains the basin of attraction for all the six stable equilibria in the set S_1. As an illustration, for any initial condition satisfying $x_2 < x(0) < \infty$, the solution $x(t)$ of $\dot{x} = f_1(x) = 1 - (1 + k_0)x$ is such that $x(t) = 1/(1 + k_0)$ which is the equilibrium E_3 in Table 3. Similar convergence results hold for the rest of the five stable equilibria in S_1.

TABLE 3. Distribution and stability of equilibria for $f(x)$ in (3.1) Recall that $x_1 \approx 0.0352$ and $x_2 \approx 0.3850$, a_i^* denotes a large positive real number. λ *denotes an eigenvalue of the Jacobian of* $f(x)$ *at the equilibria.*

Case	Parameter values	Equilibria	λ	Stability	Basin at attraction
	$k_0 = 0$	$E_1 = x_1$	$-a_1^*$	E_1; Stable–chatter	
1	$k_1 = 35$	$E_2 = x_2$	a_2^*	E_2; Unstable	
		$E_3 = \frac{1}{(1+k_0)}$	-1.0	E_3; Stable	(x_2, ∞)
	$k_0 = 0$	$E_4 = \frac{1}{(1+k_1)}$	-11.0	E_1; Stable	(x_1, x_2)
2	$k_1 = 10$	$E_5 = x_2$	a_3^*	E_2; Unstable	
		$E_6 = \frac{1}{(1+k_0)}$	-1.0	E_3; Stable	(x_2, ∞)
3	$k_0 = 0$ $k_1 = 1$	$E_7 = \frac{1}{(1+k_0)}$	-1.0	E_1; Stable	(x_2, ∞)
4	$k_0 = 30$ $k_1 = 35$	$E_8 = \frac{1}{(1+k_0)}$	-41.12	E_1; Stable	$(-\infty, x_1)$
5	$k_0 = 5$ $k_1 = 20$	$E_9 = \frac{1}{(1+k_1)}$	-21.67	E_1; Stable	(x_1, x_2)
6	$k_0 = 5$ $k_1 = 35$	$E_{10} = x_1$	$-a_4^*$	E_1; Stable–chatter[1]	

[1] Chatter refers to a special type of oscillation exhibited by a control system with a relay switch – as the one normally used in domestic heating/cooling system. While in the heating mode, if the air temperature is above (below) the threshold, the heating is turned off (on). The frequency of the on-off chatter depends on the sensitivity of the relay.

Consequently we only need to apply Filipov's Theory in Appendix B to the four cases in the set S_2. We consider two cases.

3.3. **Behavior of** (3.1) **around** x_1**.** Referring to Appendix B., let $h(x) = x - x_1$, and hence, $\frac{dh}{dx} = h_x(x) = 1$. Then (3.1) becomes

$$\dot{x} = \begin{cases} f_1(x) = 1 - (1 + k_0)\, x, & \text{if } h(x) < 0, \\ f_2(x) = 1 - (1 + k_1)\, x, & \text{if } h(x) > 0, \end{cases} \tag{3.2}$$

TABLE 4. Distribution and stability of equilibria for $f(x)$ in (3.1). Recall that $x_1 \approx 0.0352$ and $x_2 \approx 0.3850$.

Case number	Parameter values	Equilibria	λ - Eigenvalue of the Jacobian of $f(x)$ at the equilibria	Stability
1	$k_0 = 0$ $k_1 = 35$	$E_1 = 0.0373$	-154.76	E_1; Stable–chatter
		$E_2 = 0.3911$	295.98	E_2; Unstable
		$E_3 = 1.0$	-1.0	E_3; Stable
2	$k_0 = 0$ $k_1 = 10$	$E_4 = 0.0909$	-11.0	E_1; Stable
		$E_5 = 0.3883$	258.03	E_2; Unstable
		$E_6 = 1.0$	-1.0	E_3; Stable
3	$k_0 = 0$ $k_1 = 1$	$E_7 = 1.0$	-1.0	E_1; Stable
4	$k_0 = 30$ $k_1 = 35$	$E_8 = 0.0316$	-41.12	E_1; Stable
5	$k_0 = 5$ $k_1 = 20$	$E_9 = 0.0477$	-21.67	E_1; Stable
6	$k_0 = 5$ $k_1 = 35$	$E_10 = 0.0369$	-144.70	E_1; Stable–chatter

where $f_1(x_1) \neq f_2(x_1)$ since $k_0 < k_1$.

From (B.9)–(B.10), $h_x(x) = 1$, it follows that

$$\beta(x_1) = \frac{f_1(x_1) + f_2(x_1)}{f_1(x_1) - f_2(x_1)} \tag{3.3}$$

and

$$f_U(x_1) = 0. \tag{3.4}$$

Similarly, from (B.11)–(B.12), it follows that

$$\alpha(x_1) = \frac{f_1(x_1)}{f_1(x_1) - f_2(x_1)} \tag{3.5}$$

and

$$f_F(x_1) = 0. \tag{3.6}$$

In other words, by Filipov-Utkin Theory, $f(x_1) = 0$ which in turn means that the trajectory $x(t)$ starting from $x(0)$ where $-\infty < x(0) < x_1$ or

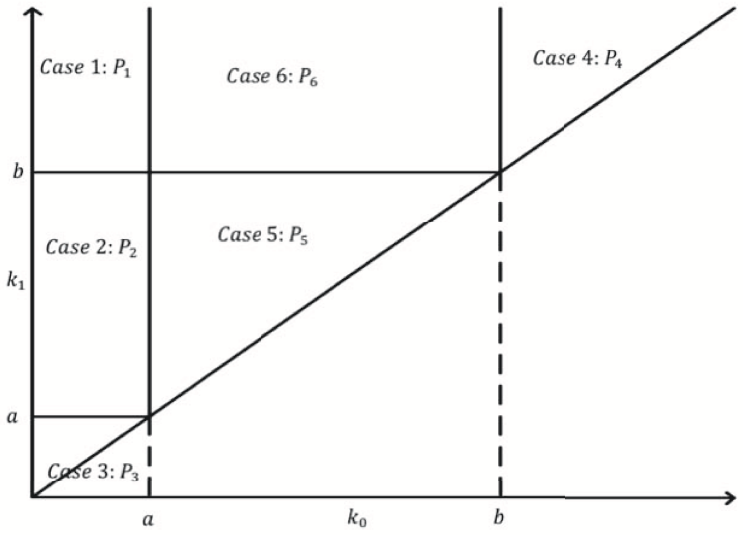

FIGURE 4. A partition of the 2-D parameter space with k_0 as x-axis and k_1 as y-axis induced by the six cases listed in Table 2. $a = (1 - x_2)/(x_2) \approx 1.597$, $b = (1 - x_1)/(x_1) \approx 27.409$. Since $k_0 < k_1$ we only need to consider the space above the 45 line where $k_0 = k_1$ completeness of the six cases in Table 2 follows from the fact that the union of the partitions P_1 through P_6 is equal to the upper half $(k_1 \geq k_0)$ of the positive quadrant of the 2-D plane.

$x_1 < x(0) < x_2$, should never reach the point x_1. From (3.4) and (3.6), it is immediate that it should remain there forever. A little reflection however reveals that x_1 is a point of discontinuity of the field $f(x)$ and x_1 by virtue of being a root of a 5th degree polynomial equation is, in general, an irrational number. Hence, the probability that the trajectory $x(t)$ will ever settle on x_1 is zero.

It can be shown (refer to Appendix C) that the trajectory $x(t)$ starting from $(-\infty, x_1)$ or (x_1, x_2) will enter a σ-neighborhood of x_1 in finite time, say k^*. Since x^- refers to points left of x and x^+ refers to points right of x, $f_1(x_1^-) > 0$ and $f_2(x_1^+) > 0$, it is immediate that the trajectory once it reaches the $\cap I'$-neighborhood of x_1 in time k^*, then for all $k > k^*$, it will oscillate between the two sides of x_1. That is x_1 corresponds to attracting

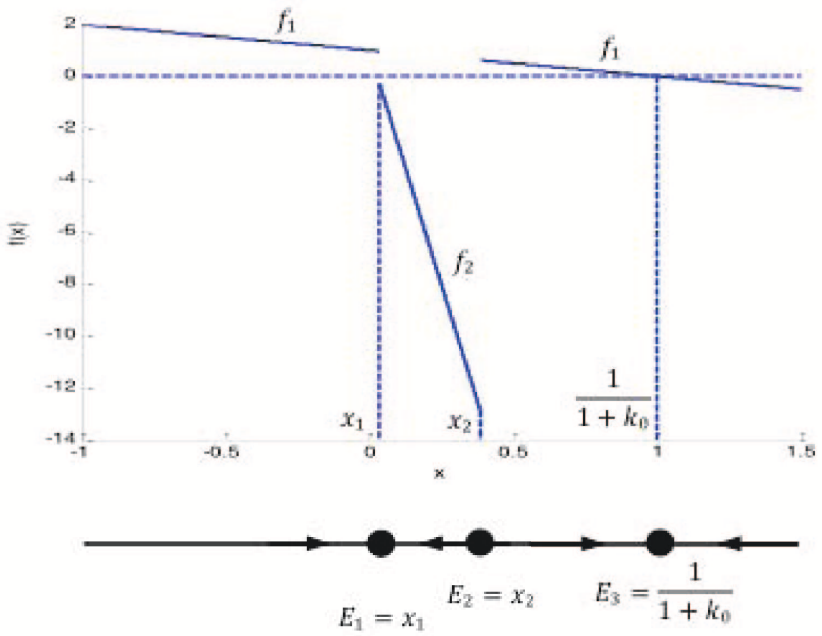

FIGURE 5. Flow field for case 1 ($k_0 = 0$ and $k_1 = 35$).

sliding regime in Appendix B. This type of oscillation is known as chatter in control literature.

The above analysis applies to equilibria E_1 and E_{10}. Refer to Figures 6 and 7 for an illustration of case 1 in Table 3.

3.4. **Behavior of** (3.1) **Around** x_2**.** By a similar analysis, using $h(x) = x - x_1$, it also follows that $f_U(x_2) = f_F(x_2) = 0$. However, since $f_1\left(x_2^+\right) > 0$ and $f_2\left(x_2^-\right) > 0$, x_2 is basically repulsive and the solution starting from (x_1, x_2) or (x_2, ∞) can never approach x_2. Hence, the equilibria E_2 and E_5 can never be reached at all.

3.5. **A Look at Bifurcation.** Referring to Figure 4, consider Case 1 when $0 \leq k_0 < a$, and $b < k_1$ with $f_1(x_1) > 0 > f_2(x_1)$, and $f_1(x_2) > 0 > f_2(x_2)$. For definiteness, let us fix k_0 to some value in the range $0 \leq k_0 < a$. This means that the shape of $f_1(x)$ is fixed. Now, consider the effect of decreasing k_1 on the shape of $f_2(x)$ from its current value $b < k_1$. When $k_1 = b$, it follows that $f_2(x_1) = 0$. That is, as the value of k_1 is moved down across b, $f_2(x_1)$ increases from being negative to positive which in

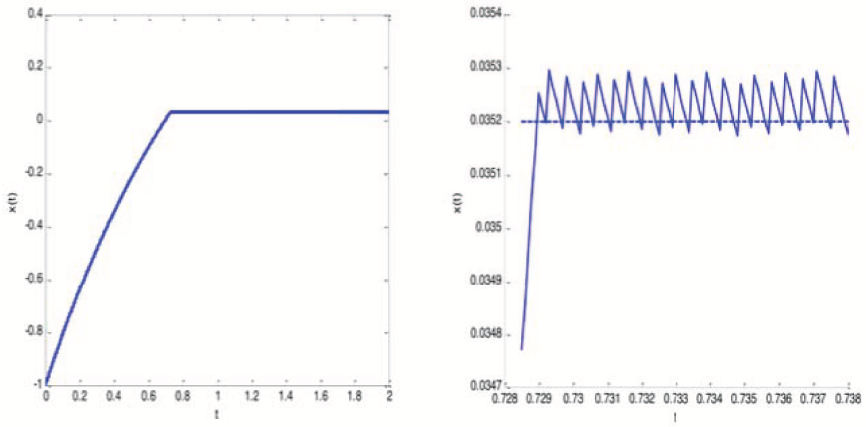

FIGURE 6. Plot of the solution $x(t)$ vs. t for $x(0) = -1$.

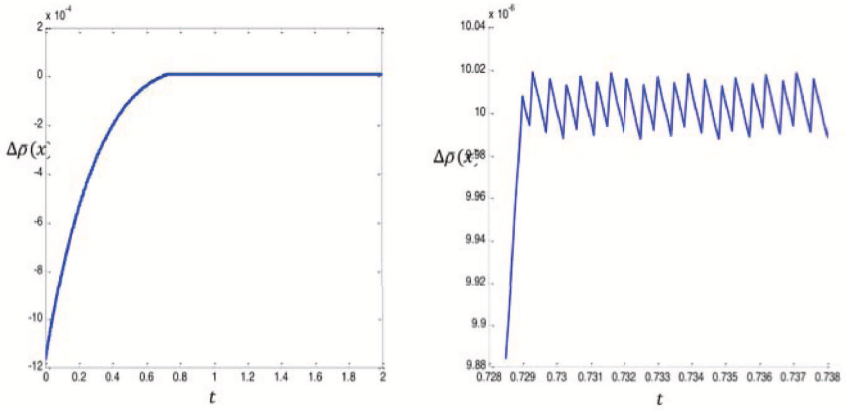

FIGURE 7. Plot of the variation of $\Delta\overline{\rho}(x)$ vs. t for $x(0) = -1$.

turn means that Case 1 morphs to Case 2 in Figure 4. Also refer to Table 2 and 3 for changes in the equilibria and their properties, when k_1 reaches down to the level $k_1 = a$, it can be verified that $f_2(x_2) = 0$. That is, as k_1 decreases across a, $f_2(x_2)$ increases from negative to positive . Thus, Case 2 morphs to Case 3 in Figure 4. Again refer to Tables 2 and 3 for changes in the number and properties of equilibria. A similar bifurcation can be demonstrated when (a) one keeps k_1 fixed and increases k_0 while keeping $k_0 < k_1$ and (b) by varying both k_0 and k_1 across a diagonal parallel to the 45° line in $k_0 - k_1$ plane in Figure 4.

TABLE 5. Equilibria for (4.1).

Equilibrium	x	Eigenvalue	Status
1	0.00552	−181.0	Stable
2	0.46280	368.9749	Unstable
3	1.0	−1.0	Stable

4. Analysis of a realistic model

Following the developments in the Appendix D, a realistic model for the temperature evolution in a two box system of pure water is given

$$\begin{aligned} \frac{dx}{ds} &= (1-x) - B^{-1}F(\mathrm{Ri})\,x \\ &= 1 - \left[1 + B^{-1}F(\mathrm{Ri})\right]x, \end{aligned} \tag{4.1}$$

where x is the normalized temperature of the upper layer and s is the normalized time, with

$$B^{-1} = 180, \tag{4.2}$$

$$F(\mathrm{Ri}) = \begin{cases} 1, & \text{for } \mathrm{Ri} < 0, \\ \left[1 - \left(\frac{\mathrm{Ri}}{0.7}\right)^2\right]^3, & \text{for } 0 \le \mathrm{Ri} \le 0.7, \\ 0, & \text{for } \mathrm{Ri} \ge 0.7, \end{cases} \tag{4.3}$$

and the Richardson number

$$\mathrm{Ri} = -4.7 \times 10^4 \Delta\overline{\rho}(x) \tag{4.4}$$

with $\Delta\overline{\rho}(x)$ is given in our Appendix A.

The equilibria for (4.1) is obtained by solving

$$g(x) = 1 - [1 + 180 \times F(\mathrm{Ri})]\,x. \tag{4.5}$$

Plot of $\mathrm{Ri}(x)$ is given in Figure 8. A listing of three equilibria and their properties are given in Table 5. The rate of change of $g(x)$ around the two equilibria differ by two orders of magnitude and hence the system (4.1) exhibits stiff behavior. The evolution of $x(t)$ when (4.1) is solved by the standard stiff solver, is given in Figure 9.

5. Conclusions

In this paper we have analyzed two types of nonlinear models for the evolution of the (scaled) temperature of the top layer of a two layered system as a model for pure water lakes. First, we provide a complete characterization of the bifurcation of the flip-model with discontinuous right-hand side

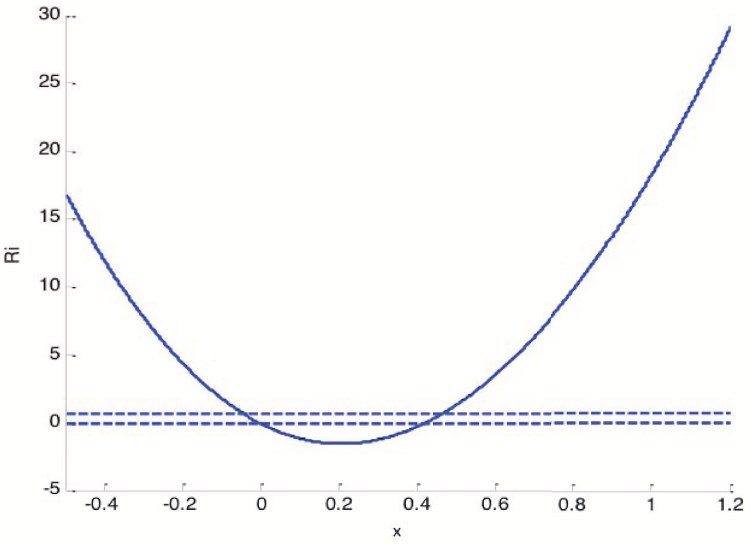

FIGURE 8. The plot of Ri vs. x.

and exhibit cases which can be oscillations. Second, using a more realistic parameterization of the vertical mixing, we described a family of stiff models that does not exhibit oscillations.

The original mixed-layer model of Price et al. [7] utilized a discontinuous mixing function which could produce oscillations that are related to the discontinuity. These would be expected to disappear under a continuous mixing function provided the numerical integration technique can handle the stiffness of the system.

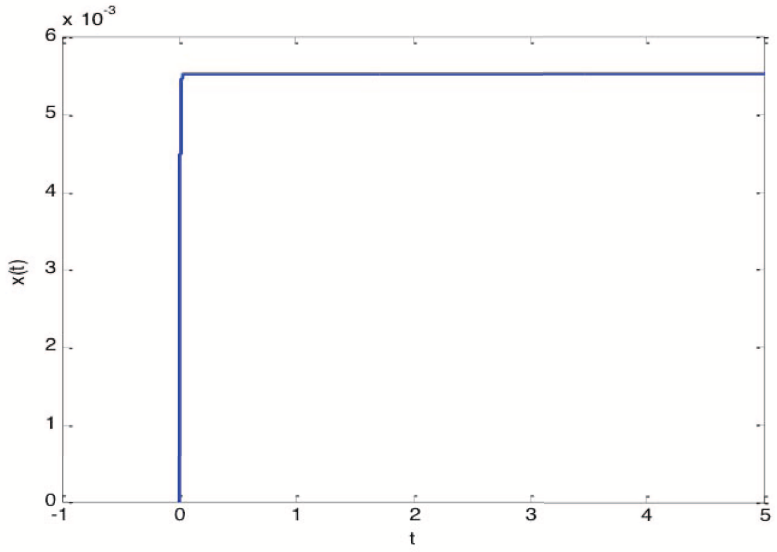

FIGURE 9. Plot the solution of (4.1) with initial condition $x_0 = 0$.

APPENDIX A. VARIATION OF DENSITY OF PURE WATER

Following the Appendix A in Gill [4], the dependence of density $\rho(T)$ of pure water on temperature T is given by the 5th order polynomial

$$\rho(T) = \sum_{i=0}^{5} a_i T^i, \tag{A.1}$$

where the values of the coefficients a_i are given in Table A.1. It can be verified that $\rho(T)$ attains its maximum value of 999.9750 very near $T_o = 4\,^{\circ}\mathrm{C}$.

Define the normalized density difference $\rho(T_s)$ as

$$\Delta\rho(T_s) = \frac{\rho(T_s) - \rho(T_d)}{\rho(T_d)}, \tag{A.2}$$

where T_s and T_d are the temperature of the top and bottom layers of the two box model described in Figure 1. It is assumed that T_d is a constant and is set at $T_d = 2\,^{\circ}\mathrm{C}$.

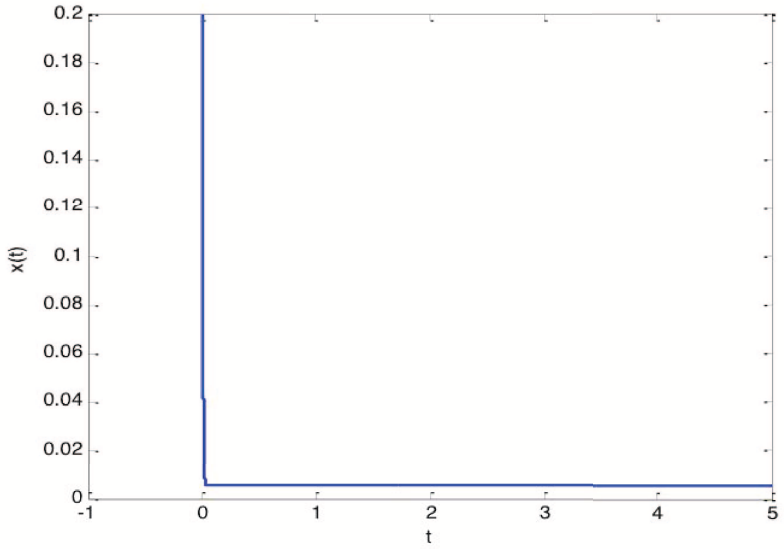

FIGURE 10. Plot the solution of (4.1) with initial condition $x_0 = 0.2$.

Let x be the non-dimensional temperature defined by

$$x = \frac{T_s - T_d}{T_a - T_d} \quad \text{or} \quad T_s = T_d + x\,(T_a - T_d)\,. \tag{A.3}$$

Substituting (A.3) in (A.1) and (A.2), we get the density in terms of x as

$$\rho\,(T_s) = \Delta\overline{\rho}\,(x) = \sum_{i=0}^{5} a_i\,[T_d + x\,(T_a - T_d)]^i, \tag{A.4}$$

and $\Delta\overline{\rho}\,(x)$ as

$$\Delta\overline{\rho}\,(x) \;= \frac{\Delta\overline{\rho}\,(x) - \;\rho\,(T_d)}{\rho\,(T_d)}. \tag{A.5}$$

A plot of $\Delta\overline{\rho}\,(x)$ vs. x for $T_a = 11.5\,^{\circ}\text{C}$ and $T_d = 2.0\,^{\circ}\text{C}$ is given Figure A.1.

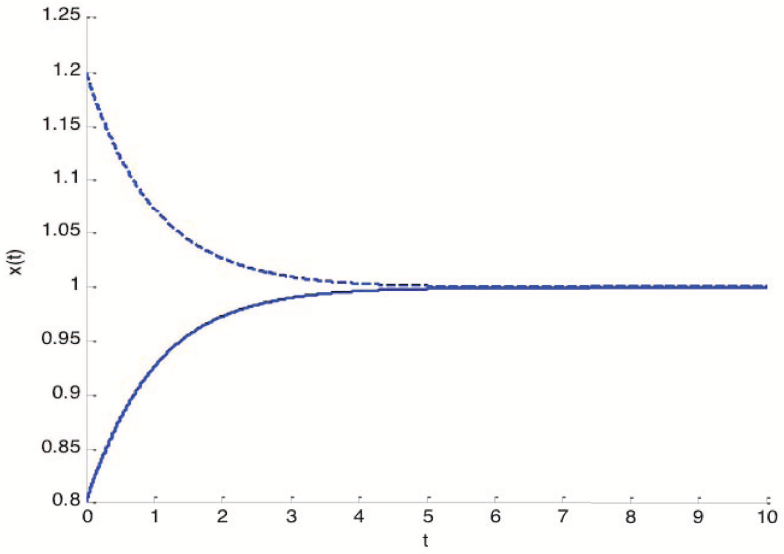

FIGURE 11. Plot the solution of (4.1) with initial conditions $x_0 = 0.8$ and $x_0 = 1.2$.

TABLE A.1. The coefficients of the polynomial in (A.1).

Coefficients	Value
a_0	$9.99842594 \times 10^{+2}$
a_1	6.793952×10^{-2}
a_2	-9.095290×10^{-3}
a_3	1.001685×10^{-4}
a_4	-1.120083×10^{-6}
a_5	6.536330×10^{-9}

APPENDIX B. PIECEWISE SMOOTH DYNAMICAL SYSTEM

This appendix provides a short summary of the literature on the theory of dynamical systems with piecewise smooth right-hand side that is relevant to the analysis of this paper. We follow very closely the developments in the recent survey paper (Section 7) by Dieci and Lopez [2] and a book (Chapter 2) by Bernardo et al. [1].

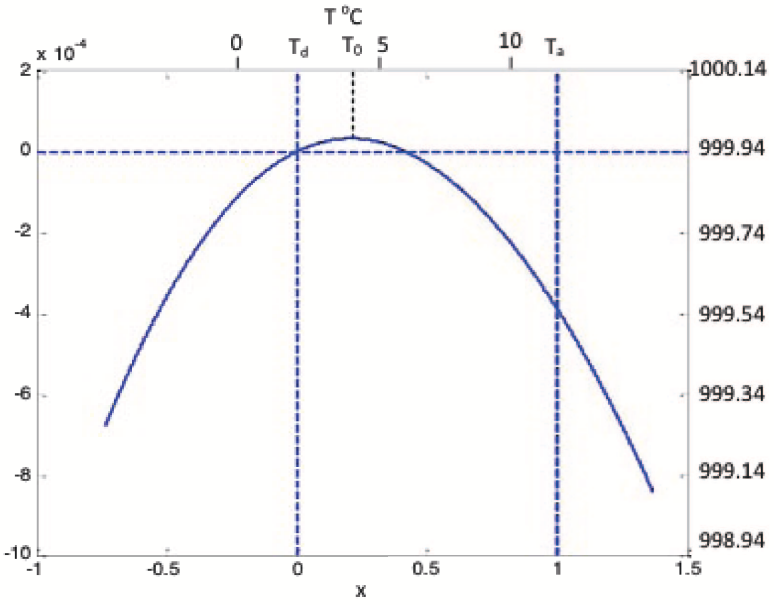

FIGURE A.1. The plot of $\Delta\overline{\rho}(x)$ vs. x.

Let $\mathbb{R}^n$ denote the state space of a dynamical system. Let $h : \mathrm{R}^n \to \mathbb{R}$ be a smooth function that defines a surface Σ in $\mathbb{R}^n$ given by

$$\Sigma = \{x \in \mathbb{R}^n | h(x) = 0\}. \tag{B.1}$$

This surface divides $\mathbb{R}^n$ into two regions

$$R_1 = \{x \in \mathbb{R}^n | h(x) < 0\} \tag{B.2}$$

and

$$R_2 = \{x \in \mathbb{R}^n | h(x) > 0\},$$

where

$$\mathbb{R}^n = R_1 \cup R_2 \cup \Sigma. \tag{B.3}$$

Let the state $x(t) \in \mathbb{R}^n$ evolve according to the piecewise smooth dynamics given by

$$\dot{x} = \begin{cases} f_1(x), & \text{if } x \in R_1, \\ f_2(x), & \text{if } x \in R_2, \end{cases} \tag{B.4}$$

where $f_i : \mathrm{R}^n \to \mathrm{R}^n$ are the smooth vector (flow) fields defined in R_i, $i = 1, 2$.

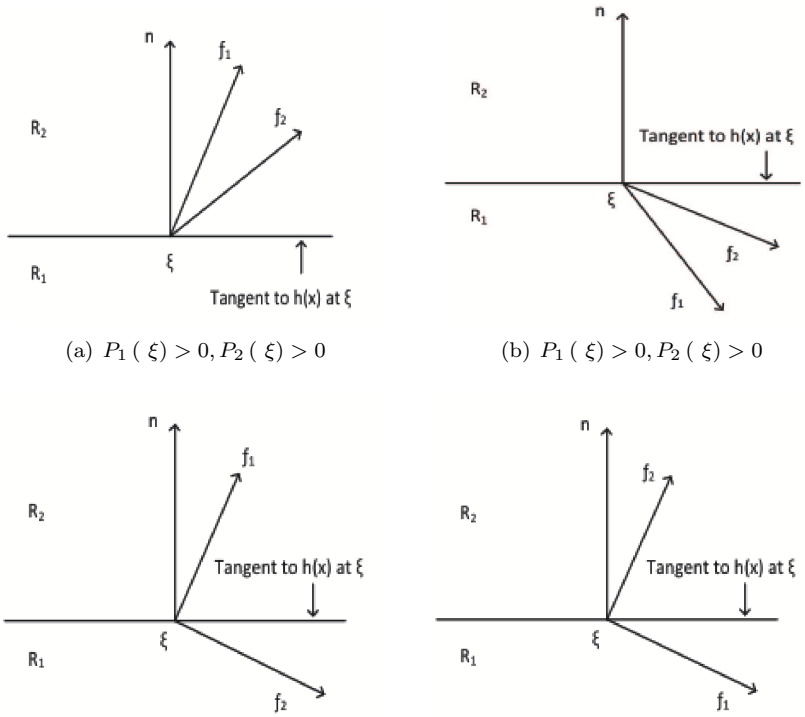

(a) $P_1(\xi) > 0, P_2(\xi) > 0$ (b) $P_1(\xi) > 0, P_2(\xi) > 0$

(c) $P_1(\xi) > 0$, $P_2(\xi) < 0$ (d) $P_1(\xi) < 0$, $P_2(\xi) > 0$

FIGURE B.1. Four possible cases. (a) and (b) define the transversal intersection, (c) and (d) define the sliding cases. Case (c) is called attractive and case (d) is called repulsive

Let $n(x) \in \mathbb{R}^n$ be the unit normal to Σ at $x \in \Sigma$ defined by

$$n(x) = \frac{h_x(x)}{\|h_x(x)\|}, \tag{B.5}$$

where $h_x(x) \in \mathbb{R}^n$ is the gradient of $h(x)$ with respect to x. Let

$$P_i(x) = n^T(x) f_i(x) \tag{B.6}$$

be the inner product that defines the orthogonal projection of the flow field $f_i(x)$ onto $n(x)$. It is assumed that $f_i(x)$ is not tangential to Σ at the point x, that is, $P_i(x) \neq 0$ at $x \in \Sigma$. Then there are exactly two possibilities: each of the $P_i(x)$ is either positive or negative.

Assuming that the solution $x(t)$ reaches $\xi \in \Sigma$ in finite time, then it will enter the region R_2 (R_1) if it starts in R_1 (R_2) and $P_1(\xi) > 0$ (< 0) since $h(x(t))$ would be increasing (decreasing) along the solution $x(t)$. Consequently, we get the following four cases as described in Figure B.1 that leads to the following classification.

(1) Transversal intersection. The trajectory $x(t)$ is said to intersect Σ at ξ transversely if

$$P_1(\xi) P_2(\xi) > 0. \tag{B.7}$$

If $P_i(\xi) > 0$ for $i = 1, 2$ as in Figure B.1 (a) the solution $x(t)$ starting from R_1 will cross into R_2. Similarly, if $P_i(\xi) < 0$ for $i = 1, 2$ as in Figure B.1 (b) the solution $x(t)$ starting from R_2 will cross into R_1.

(2) Sliding modes. This case is characterized by the condition

$$P_1(\xi) P_2(\xi) < 0 \text{ for } \xi \in \Sigma. \tag{B.8}$$

When $P_1(\xi) > 0$ and $P_2(\xi) < 0$ as in Figure B.1 (c), it is called attracting sliding mode, and it is called repulsive sliding if $P_1(\xi) < 0$ and $P_2(\xi) > 0$ as in Figure B.1 (d).

There are basically two approaches to defining the field at the point of discontinuity for the sliding modes.

Approach 1.

In Utkin's equivalent control method (Utkin [10]), we define the sliding vector field

$$f_U(x) = \frac{f_1(x) + f_2(x)}{2} - \frac{f_1(x) - f_2(x)}{2}\beta(x), \tag{B.9}$$

where

$$\beta(x) = \frac{h_x^T(f_1(x) + f_2(x))}{h_x^T(f_1(x) - f_2(x))} \tag{B.10}$$

is called the equivalent control.

Approach 2.

In Filipov's method (Filipov [**?**]), define the sliding vector field as the convex combination

$$f_F(x) = (1 - \alpha(x)) f_1(x) + \alpha(x) f_2(x) \text{ for } \xi \in \Sigma, \tag{B.11}$$

where

$$\alpha(x) = \frac{h_x^T f_1(x)}{h_x^T(f_1(x) - f_2(x))}. \tag{B.12}$$

It can be verified that

$$\beta(x) = 2\alpha(x) - 1. \tag{B.13}$$

These two approaches guarantee the existence and the uniqueness of the solution of (B.1).

It is easy to verify that both f_U and f_F are orthogonal to $n(x)$ and hence along the tangent to Σ.

Finally consider a small δ neighborhood of the surface Σ on either side as shown in the Figure B.2. If $y_0 \in R_1$ lies in this neighborhood, then y_1 is decided by $f_1(y_0)$ and the time interval t used in integration. Then y_2 is decided by $f_2(y_1)$, and so on, refer to Figure B.2 for details. Then, as $\delta \to 0$, in the limit, $\alpha(x)$ defines the fraction of the time the trajectory spends in the region S_1 (Bernardo et al. [1]).

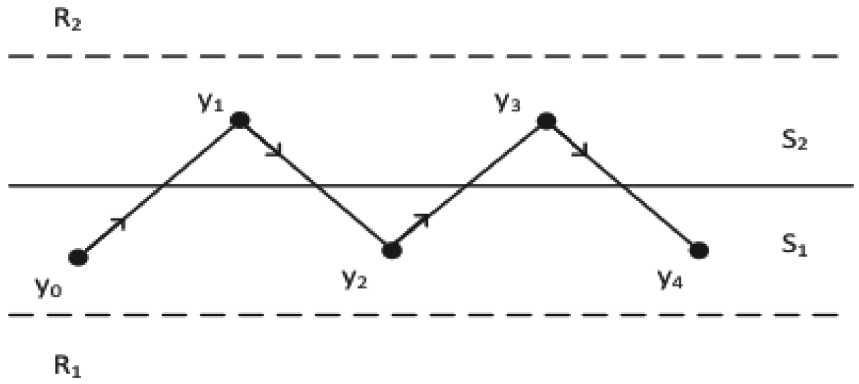

FIGURE B.2. Oscillation of trajectories in a small neighborhood S_1 and S_2 of the boundary Σ.

APPENDIX C. FINITE TIME ARRIVAL OF THE SOLUTION AT THE DISCONTINUITY x_1

Consider the ODE with DRHS given by

$$\dot{x} = \begin{cases} f_1(x) = 1 - (1 + k_0)\, x, & \text{for } x < \overline{x}_1, \text{ or } x > \overline{x}_2, \\ f_2(x) = 1 - (1 + k_1)\, x, & \text{for } \overline{x}_1 < x < \overline{x}_2, \end{cases} \tag{C.1}$$

where recall that $\overline{x}_1 \approx 0.0352$ and $\overline{x}_2 \approx 0.3850$, with an initial condition $x(0) < \overline{x}_1$. In here, we have relabeled x_1 and x_2 in Figure 2 as $\overline{x}_1$ and $\overline{x}_2$ to avoid confusion with x_k, the discretized state of (C.1).

Discretizing (C.1) using a uniform time interval > 0, we get

$$x_{k+1} = \begin{cases} m_0 x_k + \Delta, & \text{if } x < \overline{x}_1, \text{ or } x > \overline{x}_2, \\ m_1 x_k + \Delta, & \text{if } \overline{x}_1 < x < \overline{x}_2, \end{cases} \tag{C.2}$$

where

$$m_0 = 1 - (1 + k_0)\,\Delta \quad \text{and} \quad m_1 = 1 - (1 + k_1)\,\Delta. \tag{C.3}$$

Since $k_0 < k_1$, setting $\Delta < \frac{1}{1+k_1}$, it follows that $0 < m_1 < m_0 < 1$.

Iterating the first equation in (C.2), we get

$$x_k = m_0^k x_0 + \Delta \sum_{i=0}^{k-1} m_0^i. \tag{C.4}$$

Hence,

$$x^* = \lim_{k\to\infty} x_k = \Delta \sum_{i=0}^{\infty} m_0^i = \frac{\Delta}{1 - m_0} = \frac{1}{1 + k_0}. \tag{C.5}$$

Now referring to Case 1 in Table 3, we have $k_0 = 0$ and $k_1 = 35$. Hence, $x^* = 1$ is the equilibrium E_3 in this case. Consequently, if we continue integrating the first equation in (C.2), assuming that there are discontinuities at $\overline{x}_1$ and $\overline{x}_2$, we find that x_k increases monotonically from $x\,(0) < \overline{x}_1$ to the value $x^* = 1 > \overline{x}_1$. Thus, on its journey from $x\,(0)$ to x^*, the solution crosses the value $\overline{x}_1$ at some finite time, k^*.

We can indeed quantify k^*. To this end recall that $k_0 = 0$ and $k_1 = 35$ for Case 1 in Table 3. Further, in this case $m_0 = 1 - \Delta$. Hence, from (C.4), it follows that

$$x_{k^*} = \overline{x}_1 = m_0^{k^*} x_0 + \Delta \sum_{i=0}^{k^*-1} m_0^i = m_0^{k^*} x_0 + \Delta \frac{1 - m_0^{k^*}}{1 - m_0} = m_0^{k^*}\,(x_0 - 1) + 1. \tag{C.6}$$

Hence,

$$k^* = \frac{\log\,(1 - \overline{x}_1) - \log\,(1 - x_0)}{\log m_0}. \tag{C.7}$$

For the illustration in Figure 11, $x\,(0) = -1$, $\overline{x}_1 \approx 0.0352$, and $\Delta = 1 - m_0 = 0.0001$, the value of $k^* \approx 7290$, which corresponds to $t \approx 0.7290$.

When the solution $x_k < \overline{x}_1$, the one step increment is given by

$$x_{k+1} - x_k = (m_0 x_k + \Delta) - x_k = \Delta - x_k\,(1 - m_0)\,. \tag{C.8}$$

Similarly, when $x_k > \overline{x}_1$, the one step increment is given by

$$x_{k+1} - x_k = (m_1 x_k + \Delta) - x_k = \Delta - x_k\,(1 - m_1)\,. \tag{C.9}$$

Setting $x_k = \overline{x}_1 - \delta$ in (C.6) and $x_k = \overline{x}_1 + \delta$ in (C.7), it can be verified that

$$\Delta - (\overline{x}_1 - \delta)\,(1 - m_0) > \Delta - (\overline{x}_1 + \delta)\,(1 - m_1)\,, \tag{C.10}$$

or equivalently

$$(\overline{x}_1 - \delta)(1 - m_0) < (\overline{x}_1 + \delta)(1 - m_1). \tag{C.11}$$

Since

$$\frac{\overline{x}_1 - \delta}{\overline{x}_1 + \delta} < \frac{1 - m_1}{1 - m_0} = \frac{1}{1 + k_0} \leq 1, \tag{C.12}$$

it follows that the one step upward increment for iterates bellow x_1 are larger than the one step downward increment for iterates above x_1.

Appendix D. Real World Parameter

The model shown in Figure 1 is very similar to that of Ruddick and Zhang [9] as described in their Section 2, with two differences:

(1) Salinity is assumed zero in the lake, such that all mixing of heat is due to turbulence, and salt flux is zero (i.e., no double-diffusive mixing).
(2) Ruddick and Zhang [9] assume an upper layer thickness H, thermocline of thickness h and turbulent diffusivity $K = K_0 F(\mathrm{Ri})$ $[\mathrm{m\,s^{-2}}]$, where Ri is a Richardson number and K_0, is taken to be $5 \times 10^{-3}\,\mathrm{m^2\,s^{-1}}$ Large et al. [6], while the present paper assumes a sharp interface with interfacial volumetric exchange rate γ $[\mathrm{m^3/s}]$, assumed to depend on density difference.

The remaining differences are notational. Table D.1 defines and links the key parameters and variables from [9] to the present notation. We undertake three tasks: linking the forcing parameters of [9] to the present model, estimating a Richardson number, and estimating the functional dependence of mixing on a Richardson number.

Relationship to Forcing Parameters in [9].

The (dimensional) equation expressing conservation of temperature (i.e., heat) for the upper layer and thermocline is ([9, Eq. (2.7b)], multiplied by A):

$$\mathrm{HA}\frac{d}{\mathrm{dt}}(T_s - T_d) = A\frac{B^*}{\rho c_p}(T_a - T_s) - A\frac{K_0 F(\mathrm{Ri})}{h}(T_s - T_d), \tag{D.1}$$

which corresponds to Eq. (2.1) of this paper. The atmospheric exchange rate coefficient, B^*, links the net heat flux to the difference between ocean and effective atmospheric temperature, and was found by Haney [5] to be $39\,\mathrm{W\,m^{-2}\,{}^\circ C^{-1}}$, varying only 20% with latitude. In this equation, $c_p = 4186\,\mathrm{J\,kg^{-1}\,{}^\circ C^{-1}}$ is the thermal heat capacity of water and $\rho = 1000\,\mathrm{kg\,m^{-3}}$ is the water density. The unstratified diffusivity $K_0 = 5 \times 10^{-3}\,\mathrm{m^2\,s^{-1}}$.

TABLE D.1. Key variables and parameters in this paper, and their equivalents in [9].

Present Paper		[9]	
Physical Description	Quantity or symbol	Equivalent Quantity	Physical Description
Upper layer volume	V [m^3]	HA	
		H[m]	Upper layer thickness
		A[m^3]	Upper layer area
Atmospheric exchange coefficient	C_T[$m^3\,s^{-1}$]	$\frac{AB^*}{\rho c_p}$[$m^3\,s^{-1}$]	$B^* = 39\,m^{-2}\,°C^{-1}$ coefficient Haney [5]
Interfacial exchange rate	γ[$m^3\,s^{-1}$]	$\frac{AK}{h} = \frac{AK_0F(\mathrm{Ri})}{h}$	K[$m^2\,°C^{-1}$] = Turbulent diffusivity
Scaled temperature	$x = \frac{T_a - T_s}{T_a - T_d}$	$T = \frac{T_0 - T_1}{T_0 - T_2}$	[Dimensionless]
Scaled time	$s = \frac{B^*}{\rho c_p H} t$		[Dimensionless]
$\frac{\text{Relaxation time}}{\text{mixing time}}$	η	$B^{-1} = \frac{\rho c_p K_0}{B^* h}$	$\frac{\text{Forcing time}}{\text{mixing time}}$
Mixing rate function	$f(\Delta\overline{\rho}(x))$	$F(\mathrm{Ri})$	Mixing rate function

Temperature is scaled the same way in the present paper and in [9] (see Table D.1). In [9], time is scaled by the diffusion time $(H\,h)/K_0$, while in the present paper time is scaled by the atmospheric forcing time, $\rho c_p/B^*$. Conservation of temperature then becomes:

$$\frac{dx}{ds} = (1 - x) - B^{-1} F(\mathrm{Ri})\, x, \tag{D.2}$$

where

$$B^{-1} = \frac{\rho c_p K_0}{B^* h}$$

is the ratio of the atmospheric forcing time to the diffusion time—i.e., the time scale that the upper layer is warmed or cooled by the atmosphere divided by the time scale of the upper layer temperature change by mixing with the deep layer. Comparison of the above equation with (2.4) shows that $B^{-1} = \overline{\eta}$ and $F(\mathrm{Ri}) = f(\Delta\overline{\rho}(x))$. Substitution of the numerical values above, and taking H and h to be $3m$ gives $\overline{\eta} = B^{-1} = 180$.

Richardson Number Dependence.

Large et al. [6] reviewed the physics and models of upper oceanic vertical mixing, and developed a set of diffusivity parameterizations (K-Profile Parametrization, or KPP) that encompass a variety of processes and situations. While this model is fairly complicated and requires detailed numerical calculation to implement, some of the underlying concepts allow a relatively simple parameterization that allows for interfacial mixing by wind-induced and shear-induced turbulence and convective surface forcing. In this subsection we formulate a model of mixing with simple links between Ri and surface forcing so that $F\left(\mathrm{Ri}\right)$ can be related to $f\left(\Delta\overline{\rho}\left(x\right)\right)$.

The most appropriate Richardson number definition for a surface mixed layer is the bulk Richardson number, which we modify as suggested by Large et al. [6, Eq. (2)] to include both mean shear and turbulent shear near the base of the surface layer:

$$\mathrm{Ri} = g\frac{\Delta\rho}{\rho}\frac{H}{\left|\Delta\mathbf{v}\right|^2 + \left|V_t\right|^2}, \tag{D.3}$$

where ρ is the density difference, $\mathbf{v}$ is the mean velocity difference between surface and deep layers, and V_t is the turbulent velocity fluctuation. Because there is no double-diffusive mixing, the turbulent mixing is produced by the sum of surface wind stress τ and convective buoyancy flux $J = -\frac{gB^*}{\rho c_p}\left(T_a - T_s\right)$ [$\mathrm{m^2 s^{-3}}$] which is positive when the surface layer is being cooled from above. Raupach et al. [8] find that in a constant stress boundary layer the turbulent velocity is proportional to the friction velocity u^*:

$$\left|V_t\right|^2 = u^{'2} + v^{'2} + w^{'2} = 4.6u^{*2}, \tag{D.4}$$

where $u^{*2} = \left|\tau\right|/\rho$. While a surface mixed layer has stress decreasing with depth, we expect similar scaling to hold. For a convective (cooled) boundary layer, the turbulent convective velocity is assumed to follow the classic scaling (Large et al.[6, Eq. 6])

$$w^* = \left(JH\right)^{1/3}. \tag{D.5}$$

We assume the total turbulent velocity is the sum of these two forcings:

$$\left|V_t\right|^2 = 4.6u^{*2} + w^{*2} = \frac{4.6\tau}{\rho} + \left(JH\right)^{2/3}. \tag{D.6}$$

Therefore, the bulk Richardson number becomes

$$R = g\frac{\Delta\rho}{\rho}\frac{H}{\left|\Delta\mathbf{v}\right|^2 + 4.6u^{*2} + w^{*2}}. \tag{D.7}$$

For representative conditions in a lake, we take $\mathbf{v} = 0.01\,\mathrm{m\,s^{-1}}$, $\tau = 0.004\,\mathrm{N\,m^{-2}}$, appropriate to a $2\,\mathrm{m\,s^{-1}}$ wind speed, giving a friction velocity of $u^* = 0.002\,\mathrm{m\,s^{-1}}$. If we take the surface air temperature to be $2\,^\circ\mathrm{C}$ below the upper layer temperature, and $\alpha = 2 \times 10^{-4}\,^\circ\mathrm{C}$ the surface buoyancy flux is approximately $4 \times 10^{-8}\,\mathrm{m^3\,s^{-1}}$, and w* becomes $0.005\,\mathrm{m\,s^{-1}}$. The Richardson number is then related to $\overline{\rho} = (\Delta\rho)/(\rho)$ by

$$\mathrm{Ri} = -4.7 \times 10^4 \overline{\rho}. \tag{D.8}$$

The factor in (D.8) will of course vary with conditions, but the mean square shear dominates by a factor of 10 over turbulent shear in the contribution to the Richardson number, and is likely to remain relatively constant due to wind-generated internal motions.

The Mixing Parameterization.

The functional dependence of mixing rate in the KPP parameterization depends on location, having a complicated functionality within the upper mixed layer and a simpler dependence on a Richardson number beneath it. In the context of a two-layer model, we adopt the parameterization of Large et al. [6] for the region below the boundary layer:

$$\gamma = \frac{\mathrm{AK}}{h} = \frac{AK_0 F\left(\mathrm{Ri}\right)}{h}, \tag{D.9}$$

where the interface thickness $h = 3\,\mathrm{m}$, the unstratified diffusivity $K_0 = 5 \times 10^{-3}\,\mathrm{m\,s^{-1}}$ and Ri is as given above. The functional dependence F of diffusivity on a Richardson number is given by Large et al. [6] as:

$$K/K_0 = \begin{cases} 1, & \text{for } \mathrm{Ri} < 0; \\ \left[1 - \left(\frac{\mathrm{Ri}}{0.7}\right)^2\right]^3, & \text{for } 0 < \mathrm{Ri} < 0.7; \\ 0, & \text{for } \mathrm{Ri} \geq 0.7. \end{cases} \tag{D.10}$$

This behavior is discontinuous at $\mathrm{Ri} = 0$ and 0.7, and a simpler functional form that relates to the solution techniques used here is:

$$K/K_0 = F\left(\mathrm{Ri}\right) = \left[5.5 \tanh\left(\mathrm{Ri} - 0.32\right) - 1\right]/2. \tag{D.11}$$

The two functional forms are shown in the graph below, showing a smooth decrease in the range $0 < \mathrm{Ri} < 0.7$, and confirming that the tanh function is a good fit to the form suggested by Large et al. [6]. $F\left(\mathrm{Ri}\right)$ can easily be transformed to $f\left(\Delta\rho\right)$ by substituting (D.7) (or (D.8) for specific forcing) into either (D.1) or (D.11). As an example, the upper axis of the figure below shows $\Delta\rho$ from (C.11), indicating that the midpoint of the transition occurs at $\overline{\rho} = 0.015$.

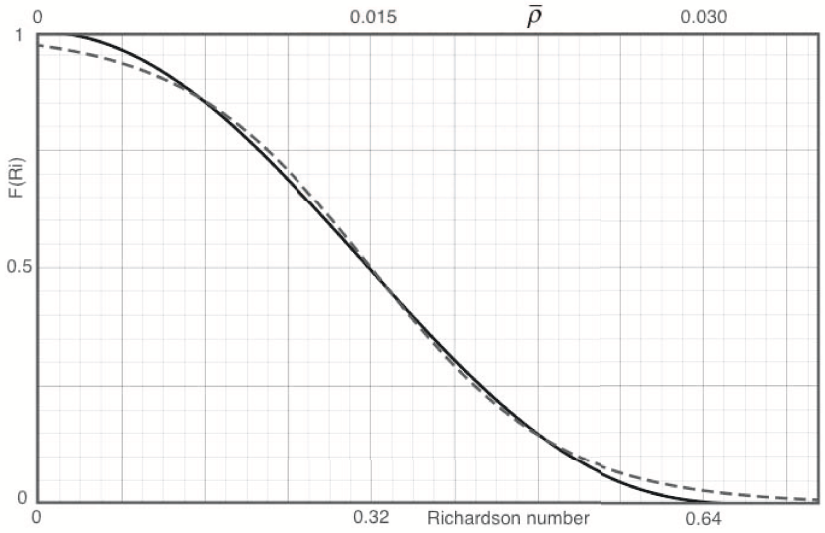

FIGURE D.1. Plot of $F(\mathrm{Ri})$ vs Ri for the functional form of Large et al. [Eq. (D.10)][6], solid black curve) and the tanh approximation above (Eq. (C.11), dashed gray curve).

REFERENCES

[1] M. Bernardo, C. Budd, A. R. Champneys, and P. Kowalczyk, *Piecewise-Smooth Dynamical Systems: Theory and Applications*, Springer, place of publication, 2008.

[2] L. Dieci and L. Lopez, *A survey of numerical methods for IVPs of ODEs with discontinuous right-hand side*, Journal of Computational and Applied Mathematics, **236** (2012), 3967–3991.

[3] A. F. Filippov, *Differential Equations with Discontinuous Righthand Sides*, Kluwer Academic Publications, place of publication, 1998.

[4] A. E. Gill, *Atmosphere-Ocean Dynamics*, Academic Press, place of publication, 1982.

[5] R. L. Haney, *Surface thermal boundary conditions for ocean circulation models*, Journal of Physical Oceanography, 1 **4** (1971), 241–248.

[6] W. G. Large, J. C. McWilliams, and S. C. Doney, *Oceanic vertical mixing: A review and a model with a nonlocal boundary layer parameterization*, Reviews of Geophysics, **32** (1994), 363–403.

[7] J. F. Price, R. A. Weller, and R. Pinkel., *Diurnal cycling: Observations and models of the upper ocean response to diurnal heating, cooling, and wind mixing*, Journal of Geophysical Research, **91** (C7) (1986), 8411–8427.

[8] M. R. Raupach, R. A. Antonia, and S. Rajagopalan, *Rough wall turbulent boundary layers*, Applied Mechanics Review, **44** (1) (1991), 1–25.
[9] B. Ruddick, and L. Zhang, *The mythical thermohaline oscillator?*, Journal of Marine Research, **47** (1989), 717–746.
[10] V. I. Utkin, *Sliding Modes in Control and Optimization*, Springer Verlag, New York, 1992.
[11] P. Welander, *A simple heat-salt oscillator*, Dynamics of Atmospheres and Oceans, **6** (1982), 233–242.

MSC2010: 34C15, 35F50
Key words and phrases: Density of pure water, vertical instability, two layered system.

School of Computer Science, University of Oklahoma,, Norman, OK 73019
E-mail address: varahan@ou.edu

School of Computer Science, University of Oklahoma,, Norman, OK 73019
E-mail address: trung.nguyen@ou.edu

Department of Oceanography, Dalhousie University, Halifax, Nova Scotia, B3H 4R2, Canada
E-mail address: barry.ruddick@dal.ca